

# Energy spectrum of turbulent fluctuations in boundary driven reduced magnetohydrodynamics

Pablo Dmitruk<sup>1</sup>, Daniel O. Gómez<sup>2</sup> and William H. Matthaeus<sup>1</sup>

<sup>1</sup>*Bartol Research Institute, University of Delaware, Newark, DE 19716*

<sup>2</sup>*Departamento de Física, Facultad de Ciencias Exactas y Naturales, Universidad de Buenos Aires, Ciudad Universitaria, 1428 Buenos Aires, Argentina*

## Abstract

The nonlinear dynamics of a bundle of magnetic flux ropes driven by stationary fluid motions at their endpoints is studied, by performing numerical simulations of the magnetohydrodynamic (MHD) equations. The development of MHD turbulence is shown, where the system reaches a state that is characterized by the ratio between the Alfvén time (the time for incompressible MHD waves to travel along the field lines) and the convective time scale of the driving motions. This ratio of time scales determines the energy spectra and the relaxation toward different regimes ranging from weak to strong turbulence. A connection is made with phenomenological theories for the energy spectra in MHD turbulence.

## I. INTRODUCTION

The search for universal scaling properties in magnetohydrodynamic turbulence, of the type developed by Kolmogorov [1] for hydrodynamic turbulence, has been the subject of many theoretical and numerical studies, since the pioneering phenomenological arguments put forward independently by Iroshnikov and Kraichnan [2,3] (hereafter IK). The phenomenological arguments of Kolmogorov, which give rise to the famous power law  $E_k \sim k^{-5/3}$  for the omnidirectional energy spectrum  $E_k$  in terms of the wavenumber  $k$ , were modified by IK to include magnetic field effects, deriving an energy spectrum power law like  $E_k \sim k^{-3/2}$ . An alternative point of view, however, was proposed [4] indicating that the original Kolmogorov scenario is still applicable in certain cases to MHD as well as to hydrodynamics. Along similar lines, a phenomenological theory was proposed in Ref. [5] for a steady inertial range spectral law that reduces to the IK and Kolmogorov laws in appropriate limits. To distinguish between the two power laws is a difficult task both observationally and numerically [6], partly because the power law indexes are too close, but also because assumptions on the theories, such as homogeneity, isotropy and time stationarity are often lost.

For instance, when a strong, externally supported, magnetic field is present, the key assumption of isotropy breaks down. It has been shown [7–10] that the cascade renders itself anisotropic, and that the spectrum in the direction of the magnetic field becomes strongly suppressed. This situation also holds for compressible MHD, where a variance anisotropy is also found [11], i.e., components of the fluctuating fields in the strong magnetic field direction are small compared to the transverse components. On theoretical grounds, this configuration has been found [12] to be appropriately described, in the low-frequency limit, by the so called Reduced MHD [13,14] approximation (RMHD).

Phenomenological theories alternative to the IK scenario [2,3] when a strong magnetic field is present have been also presented to describe the perpendicular spectrum in anisotropic conditions [15,9]. Recently, a formal closure model has been introduced, which obtains a

kinetic equation for the anisotropic energy spectrum in the limit known as *weak MHD turbulence* [16].

Besides the anisotropy introduced by a strong magnetic field, another effect that may modify the cascade situation is the presence of driving boundaries. We intend to address the effect of both a strong external magnetic field and the driving boundaries on MHD turbulence, by considering the particular case of a plasma under a strong uniform field in the  $z$ -direction, limited within the transverse planes  $z = 0$  and  $z = L_z$  where an imposed velocity field is applied. This case is inspired in the theoretical model of a coronal magnetic loop, which is forced through convective motions at its footpoints. Such a model loop, proposed in Ref. [17], has been widely studied in many different contexts, although not necessarily in a turbulent scenario. Most studies address the issue of current sheet formation [18–20], non-steady reconnection [21,22] and coronal heating [23,24,21,25,26]. However, this paper is not aimed at studying the dynamics of coronal magnetic loops. Instead, we focus our analysis on the (steady) perpendicular energy spectrum of boundary driven RMHD and make a connection with the phenomenological theories of MHD turbulence. We pay particular attention to the issues of numerical resolution required to yield well resolved turbulent spectra from direct numerical simulations.

The organization of the paper is as follows: in section II we present our model and the RMHD equations. Section III contains a description of the boundary conditions and the numerical code. Section IV describes the statistically steady regime and the dissipation rate scaling law. In Section V we show the numerically obtained energy spectra and discuss the connection with phenomenological theories of turbulence. Issues of numerical resolution are also addressed. Section VI discusses the typical dissipative structures. Section VII contains the conclusions.

## II. MODEL AND EQUATIONS

Let us assume a low- $\beta$  magnetofluid ( $\beta$  is the ratio of gas pressure to magnetic pressure) permeated by an initially uniform magnetic field  $\mathbf{B} = B_0 \hat{\mathbf{z}}$ , which is elongated along the  $\hat{\mathbf{z}}$ -direction (i.e.  $L_z \gg L_\perp$ ), as shown in Figure 1. Under these conditions, the so-called reduced magnetohydrodynamic equations (RMHD) are applicable [13,14,12] to describe the dominant low-frequency non-linear motions. Within this approximation, the magnetic and velocity fields are both divergence-free and can be expressed as

$$\mathbf{B} = B_0 \hat{\mathbf{z}} + \nabla_\perp \times (a \hat{\mathbf{z}}) \quad (1)$$

$$\mathbf{u} = \nabla_\perp \times (\psi \hat{\mathbf{z}}) \quad (2)$$

where  $a(x, y, z, t)$  is the magnetic flux function and  $\psi(x, y, z, t)$  is the stream function. The RMHD equations in terms of these scalar potentials are:

$$\partial_t a = v_A \partial_z \psi + [\psi, a] + \eta \nabla_\perp^2 a \quad (3)$$

$$\partial_t w = v_A \partial_z j + [\psi, w] - [a, j] + \nu \nabla_\perp^2 w \quad (4)$$

where  $w(x, y, z, t) = -\nabla_\perp^2 \psi$  is the parallel vorticity and  $j(x, y, z, t) = -\nabla_\perp^2 a$  is the parallel current density. The coefficient  $v_A = B_0 / \sqrt{4\pi\rho}$  is the Alfvén speed,  $\nu$  is the kinematic viscosity and  $\eta$  is the magnetic diffusivity. The non-linear terms in these equations are expressed in terms of standard Poisson brackets, i.e.  $[u, v] = (\partial_x u)(\partial_y v) - (\partial_y u)(\partial_x v)$ .

This particular theoretical setup is relevant to several plasma applications, ranging from tokamaks to magnetic loops in the solar corona. The RMHD framework has been used to study the dynamics of coronal loops in solar active regions [23,19,21,25]. The axial (and approximately constant) magnetic field in these loops has both ends or footpoints anchored in the solar photosphere. The photosphere is a high- $\beta$  plasma, which is also convectively turbulent. These convective motions at the photosphere, in turn move the magnetic fieldlines around, and drive the coronal part of the loops into a rather complex dynamical scenario.

We specify the velocity fields at the boundaries as

$$\psi(z=0)=0, \quad \psi(z=L_z)=\Psi(x,y) \quad (5)$$

where  $\Psi(x,y)$  is the stream function which describes stationary and incompressible footpoint motions. The strength of this external velocity field is proportional to a typical velocity  $U_p$ .

To transform equations (3)-(4) into their dimensionless form, we choose  $l_p = L_\perp/(2\pi)$  and  $L_z$  as the units for transverse and longitudinal distances. Since the dimensions of all physical quantities involved in these equations can be expressed as combinations of *length* and *time*, let us choose  $t_A \equiv L_z/v_A$  as the time unit. The dimensionless RMHD equations are:

$$\partial_t a = \partial_z \psi + [\psi, a] + \frac{1}{S} \nabla_\perp^2 a \quad (6)$$

$$\partial_t w = \partial_z j + [\psi, w] - [a, j] + \frac{1}{R} \nabla_\perp^2 w \quad (7)$$

where  $S^{-1} = \frac{\eta t_A}{l_p^2}$  and  $R^{-1} = \frac{\nu t_A}{l_p^2}$  are the (dimensionless) magnetic and kinetic dissipation coefficients. Hereafter, we will consider the case  $S = R$ , and thus the (common) dissipation coefficient will be the only dimensionless parameter explicitly present in equations (6)-(7) .

### III. DESCRIPTION OF THE CODE AND BOUNDARY DRIVING

We numerically integrated equations (6)-(7). To this end,  $\psi$  and  $a$  are expanded in Fourier modes in each  $(x,y)$  plane ( $0 \leq x,y \leq 2\pi$  and  $0 \leq z \leq 1$ ). The corresponding Fourier coefficients  $\psi_{\mathbf{k}}(z,t)$  and  $a_{\mathbf{k}}(z,t)$  are evolved in time using a semi-implicit scheme: linear terms are treated in a fully implicit fashion, while nonlinear terms are evolved using a second order Runge-Kutta scheme. Also, nonlinear terms are evaluated following a 2/3 fully dealiased (see Ref. [27]) pseudo-spectral technique.

To compute  $z$ -derivatives we use a standard method of finite differences in a staggered regular grid (see for instance Refs. [13,19]) of  $N_z+1$  points. The stream function is computed

on points  $z_i = i/N_z$  ( $i = 0, \dots, N_z$ ), while the magnetic flux function is computed on  $z_{i+1/2} = (i + 1/2)/N_z$  ( $i = 0, \dots, N_z - 1$ ). Boundary conditions for the stream function  $\psi$  are given at the plates  $z = 0$  and  $z = 1$ . Therefore, equation (7) is not integrated on these planes, but it is evolved in time in all the internal gridpoints  $z_i = i/N_z$  ( $i = 1, \dots, N_z - 1$ ).

We specify the stream function in equation (5) as

$$\begin{aligned} \Psi_{\mathbf{k}} &= \Psi_0 = t_A/t_p, & \text{if } 3 < k l_p < 4 \\ \Psi_{\mathbf{k}} &= 0 & \text{elsewhere} \end{aligned} \tag{8}$$

This expression imitates a stationary pattern of eddy motions of diameters between  $L_\perp/4$  and  $L_\perp/3$ , rotation speeds  $U_p$  and typical turnover times  $t_p = l_p/U_p$ . Our choice of this narrowband and non-random forcing ensures that the broadband energy spectra that we obtain are exclusively determined by the nonlinear nature of the MHD equations.

The strength of the external driver is quantified by the dimensionless factor  $\Psi_0 = t_A/t_p$  in equation (9), which is given by the ratio of the Alfvén time of the system (i.e. the response time to an impulse applied at the boundary) to the timescale of the driver itself (i.e. the eddy turnover time). Note that the velocity fields that we are imposing at the boundaries are stationary. For non-stationary footpoint motions, which might for instance represent wave activity or time-correlated random flows, other timescales should be considered in connection with the driver.

#### IV. STATIONARY REGIMES AND SCALING LAW

As mentioned in Section 2, the dissipation coefficient  $S$  (with  $S = R$ ) is the only dimensionless parameter present in equations (6)-(7). Just as important is the dimensionless factor  $t_A/t_p$  introduced by the external force applied at the boundary. Therefore, we are left with these two dimensionless numbers to characterize the solutions of the RMHD equations [i.e. equations (6)-(7) with the boundary condition given by equation (5) and equation (9)].

From purely dimensional considerations, we know that for any physical quantity, its

dimensionless version  $Q$  should be an arbitrary function of the only two dimensionless parameters of the problem, i.e.

$$Q = \mathcal{F}(Q_1, Q_2), \quad Q_1 = \frac{t_A}{t_p}, \quad Q_2 = S \quad (9)$$

For instance, for the dissipation rate per unit mass  $\epsilon$

$$Q = \epsilon \frac{t_A^3}{l_p^2} = \mathcal{F}\left(\frac{t_A}{t_p}, S\right) \quad (10)$$

A sequence of numerical simulations for different values of the dissipation coefficient performed in Ref. [25] (see also Ref. [28]), indicated that the dependence of the dissipation rate with  $S$  is rather mild. This relative insensitivity of the dissipation rate with the dissipation coefficient is consistent with similar results obtained from experiments in purely hydrodynamic turbulence [29–31]. It is also consistent with one of Kolmogorov’s hypothesis for statistically steady turbulent regimes at very large Reynolds numbers, which assumes that the dissipation rate remains finite in the limit of vanishing viscosity [31]. Therefore, if we assume that the dissipation rate in statistically steady turbulent regimes in RMHD is approximately independent of the dissipation coefficient  $S$ , we readily obtain that the dissipation rate will only depend on the time ratio  $t_A/t_p$ . A second series of simulations [25], in this case for different values of the ratio  $t_A/t_p$ , led to the following expression for the function  $\mathcal{F}$ ,

$$\epsilon = \frac{l_p^2}{t_A^3} \left(\frac{t_A}{t_p}\right)^s, \quad s = 1.51 \pm 0.04 \quad (11)$$

In the present paper, we performed numerical simulations of equations (6)-(7) with  $S = 2000$  and different values of the ratio  $t_A/t_p$  in the range  $[0.1, 1]$ . Note that  $t_A/t_p$  can also be written as  $t_A/t_p = (L_z/l_p)/(v_A/U_p)$ . For consistency with the RMHD approximation, both  $L_z/l_p$  and  $v_A/U_p$  should remain much larger than unity. However, as mentioned above, the only relevant parameter in this problem is  $t_A/t_p$ , which is free to take any value. An additional simulation with  $t_A/t_p = 2$  and  $S = 800$  is also performed. Numerical resolution ranges from  $256 \times 256 \times 64$  to  $2048 \times 2048 \times 128$  gridpoints. A Beowulf PC cluster is employed

to perform those runs, and a parallel RMHD code has been designed. Since finite-differences are used in the  $z$ -direction, while a pseudospectral method is employed for the transverse directions, a very efficient parallelization is achieved by performing the transverse gradients locally in each machine, while employing communication between machines only to perform the  $z$ -derivatives. The typical behavior of the magnetic and kinetic energy as a function of time is shown in the top panel of Figure 2, while the bottom panel shows the dissipation rate for the particular case of  $t_A/t_p = 0.5$  with  $256 \times 256 \times 64$  resolution. After an initial transient, the dissipation rate is seen to approach a statistically steady level.

## V. ENERGY SPECTRA

Energy spectra of turbulent fluctuations are essential both for phenomenological and statistical theories of MHD turbulence. We compute the perpendicular spectra at each plane and integrate in  $z$  to obtain a *perpendicular spectrum*,

$$E_{k_\perp} = \frac{1}{2} \int \sum_{k_\perp < k_x^2 + k_y^2 < k_\perp + \Delta k} [ |\mathbf{b}(k_x, k_y, z)|^2 + |\mathbf{u}(k_x, k_y, z)|^2 ] dz \quad (12)$$

where the total energy can be obtained as  $E = \int E_{k_\perp} dk_\perp$ .

As we have pointed out in the previous section, the system reaches an approximately steady state where the forcing is compensated by dissipation (Figure 2 bottom). The first stage of the system evolution is followed using a low resolution simulation. Once the steady state is achieved, a higher resolution simulation is started, by taking the Fourier coefficients from the previous run and padding the additional high  $k$  coefficients to zero. After a short transient, those additional coefficients are populated by the nonlinear cascade in a few eddy turnover times. In this way, a high resolution steady state spectrum is obtained in a relatively shorter computer time. The high resolution runs ( $2048 \times 2048 \times 64$ ) are however computationally demanding, even for runs of a few eddy turnover times.

In Figure 3 we show the magnetic and kinetic energy perpendicular spectra for different values of the quantity  $t_A/t_p$ . The right panel plots show the compensated spectra (magnetic



plus kinetic), which allow determination of the power law index  $\alpha$  observed in the inertial range where  $E_{k_\perp} \sim k_\perp^{-\alpha}$ . A first clear result observed in these plots is that the power law index depends on the value of  $t_A/t_p$ . For low values of  $t_A/t_p$  a rather steep spectra ( $\alpha > 2$ ) is observed. At intermediate values of  $t_A/t_p$  the power law index is approximately equal to  $\alpha = 2$ . For larger values of  $t_A/t_p$  the spectral law becomes flatter ( $\alpha < 2$ ). As shown in Figure 4, when  $t_A/t_p = 2$  a value close to  $\alpha = 5/3$  is obtained. For this last simulation a lower value of  $S = 800$  has to be employed, in order to have a well resolved spectrum (see discussion below).

Phenomenological theories [15,32] and a more formal theory based on closures [16] have been proposed to explain a  $k^{-2}$  spectra in a regime known as the *weak turbulence* limit. An alternative phenomenological derivation of this power law can be done using the general approach proposed in Ref. [5] in terms of the triple correlation time. The energy supply  $\epsilon$  is assumed to be equal to the  $k$ -independent spectral transfer rate. As stated in Ref. [5], if  $\tau_3(k)$  is the time scale for decay of triple correlations, which induce the spectral transfer to wavenumbers higher than  $k$ , then [3,5]

$$\epsilon \sim \tau_3(k) \frac{k E_k}{\tau_{nl}^2(k)} \quad (13)$$

where  $\tau_{nl}(k) \sim (k u_k)^{-1}$  is the non-linear time. Equation (13) implies a spectral transfer time  $\tau_s \sim \tau_{nl}^2/\tau_3$ . If  $\tau_3(k) \sim \tau_{nl}(k)$  and equipartition between magnetic and kinetic energy is assumed  $E_k^b \sim E_k^u \sim u_k^2/k$ , the usual  $E_k \sim k^{-5/3}$  Kolmogorov scaling is recovered. When  $\tau_3(k) \sim \tau_A(k) = (k \bar{b})^{-1}$ , where  $\bar{b}$  is the rms of magnetic fluctuations, and isotropy and equipartition is assumed, the IK scaling  $E_k \sim k^{-3/2}$  is obtained. If there is a strong external magnetic field the energy cascade is anisotropic and  $\tau_{nl} \sim (k_\perp u_{k_\perp})^{-1}$ . For this case, the appropriate triple correlation time  $\tau_3$  is the Alfvén wave crossing time (in the direction of the external field)  $\tau_3 \sim t_A = L_z/V_A$ , a fixed external quantity independent of  $k_\perp$  (this is different from the  $k$ -dependent Alfvén time  $\tau_A(k)$  associated with fluctuations in an isotropic situation). Again assuming equipartition,

$$\epsilon \sim t_A k_\perp E_{k_\perp} k_\perp^2 u_{k_\perp}^2 \sim t_A k_\perp^4 E_{k_\perp}^2 \quad (14)$$

and a  $E_{k_\perp} \sim k_\perp^{-2}$  spectra is obtained. This is equivalent to the wave packet interaction approach presented in Ref. [15], based on the IK scenario [2,3] but under strong anisotropic conditions. It is also interesting that an essentially similar argument [33] has been applied to the case of purely hydrodynamic turbulence in the presence of strong rotation, where the triple correlation time is set equal to a fixed external timescale  $\tau_3 \sim t_\Omega = 1/\Omega$ . This suggests an analogy between strong rotating turbulence and RMHD (i.e. MHD turbulence with a strong mean field). The simulations presented here show that the *weak limit* regime of  $E_{k_\perp} \sim k_\perp^{-2}$  is obtained when  $t_A/t_p \approx 1/2$ . For larger values of this timescale ratio, the energy spectrum approaches a Kolmogorov-like regime  $E_{k_\perp} \sim k_\perp^{-5/3}$ .

For the small  $t_A/t_p = 0.1$  case the spectrum is  $E_{k_\perp} \sim k_\perp^{-2.4}$  which would indicate that the weak turbulence regime gave rise to a regime in which the perpendicular cascade is suppressed even more. In these numerical experiments we have kept the value of  $S = l_p^2/(\eta t_A)$  fixed, while changing the value of  $t_A/t_p = (L_z U_p)/(l_p v_A)$ . If we consider that all parameters are fixed, except for  $U_p$ , we can interpret these runs as different evolutions of the system when varying the intensity  $U_p$  of the boundary driving. The result is that as the driving intensity is enhanced (i.e. larger  $t_A/t_p$ ), the spectrum becomes flatter and the regime goes through weak turbulence to a strong Kolmogorov-like state. As shown by Figure 3 (left panels), the kinetic energy spectrum is always smaller than the magnetic energy spectrum and the ratio  $E_k^u/E_k^b$  is smaller (especially at the low  $k$  structures) when the forcing is weaker.

The phenomenological argument expressed by equation (13) can be modified to address the very weak forcing case. For that case, the energy at the low and intermediate  $k$  values is essentially magnetic  $E_{k_\perp} \approx E_{k_\perp}^b$  (see Figure 3). For the non-linear time  $\tau_{nl}(k) \sim (ku_k)^{-1}$ , we replace the  $k$ -dependent velocity  $u_k$  by a constant which we expect to be of the order of the imposed boundary weak velocity  $U_p$  (i.e.  $\tau_{nl} \sim (k_\perp U_p)^{-1}$ ). A scale invariant characteristic speed corresponds to a kinetic energy spectrum  $E_{k_\perp}^u \sim k_\perp^{-1}$ . Again assuming  $\tau_3 \sim t_A$  in equation (13) we find,

$$\epsilon \sim t_A k_\perp E_{k_\perp}^b k_\perp^2 U_p^2 \quad (15)$$

and a steep spectrum  $E_{k_\perp}^b \sim k_\perp^{-3}$  is obtained. We should note that there are theoretical developments predicting spectra steeper than  $k^{-2}$ , due to nonlocal effects [15], or due to high values of the correlation between magnetic and velocity fields [34]. The latter one corresponds to  $\langle u^2 \rangle \sim \langle b^2 \rangle$ , a situation that would not be applicable for the present case. The effects of the finite values of  $S$  considered here are also expected to be more important for very weak forcing.

Phenomenologies [15] and closures [16] are also usually presented in terms of the Elsasser fields  $\mathbf{z}^\pm = \mathbf{u} \pm \mathbf{b}$ , so for completeness we computed the corresponding perpendicular spectra

$$E_{k_\perp}^\pm = \frac{1}{4} \int \sum_{k_\perp < k_x^2 + k_y^2 < k_\perp + \Delta k} |\mathbf{z}^\pm(k_x, k_y, z)|^2 dz \quad (16)$$

The results for the cases  $t_A/t_p = 0.1, 0.5, 1$  are shown in Figure 5. The compensated spectra for the product  $E_{k_\perp}^+ E_{k_\perp}^-$  are shown on the right panels of Figure 5. Weak turbulence theory [16] predicts an index  $\alpha = 4$ , which for this particular problem corresponds again approximately to the case  $t_A/t_p = 1/2$ . A higher power index  $\alpha \sim 4.9$  is instead obtained for the very weak forcing case  $t_A/t_p = 0.1$ .

A rather technical but important issue when determining spectra is whether the dissipation range is well resolved. We have considered here an exact laplacian dissipation term in the dynamical equations (i.e. no hyperviscosity is used) which makes harder to achieve higher spatial resolutions. An example from a simulation with  $t_A/t_p = 1$  is shown in Figure 6. A  $k$ -dependent Reynolds number is computed as  $R_k = u_k/(k \nu) = \sqrt{(E_k^u/k)}/\nu$ . The dissipative region in  $k$ -space is characterized by  $R_k \sim 1$ . The fact that  $R_k$  reduces monotonically and falls below unity at the largest values of  $k$ , is compelling evidence that the dissipation range is well resolved in our simulations. Similar results are obtained for the different values of  $t_A/t_p$ , although higher perpendicular resolution is required as this value is increased. For  $t_A/t_p = 2$  the excessive computational requirement has forced us to consider a lower value of  $S = 800$  to resolve the dissipation range. Another direct resolution study is shown in Figure 7 where different perpendicular spatial resolutions have been adopted for a simulation with  $t_A/t_p = 0.1$ . What this figure shows is that the spectrum is better resolved

and extends to higher wavenumbers as the resolution is increased. However, a very good picture of the lower  $k$  part of the spectra can still be obtained with the low resolution runs.

## VI. SPATIAL STRUCTURES

Figure 8 is a cross section of the simulation box (perpendicular to the strong external magnetic field) showing the spatial distribution of electric current density (z-component) at  $t = 120t_A$  for the cases  $t_A/t_p = 0.1$  (Figure 8a) and  $t_A/t_p = 0.5$  (Figure 8b). Intense positive z currents correspond to white regions, while intense negative z current concentrations are indicated in black. The current density structures extend in the z-direction (not shown) with almost no variation (as consistent with the RMHD approximation) in a current sheet-like form. These structures are highly dynamic in the  $x, y$  plane and evolve in time. They indicate the presence of multiple reconnection events (where the reconnecting magnetic field lies in the plane perpendicular to the external field) occurring within the turbulent non-linear dynamics.

The minimum thickness that current sheets can reach is determined by the magnetic diffusivity. In numerical simulations of turbulent regimes, the magnetic diffusivity is usually made as small as possible, in such a way that the sheet thickness (which is about the smallest spatial feature expected in these simulations) is just marginally resolved. The two cases presented in Figure 8 share the same value of magnetic diffusivity ( $S = 2000$ ), and in fact it is possible to find very narrow current sheets in both cases, close to the resolution limit. Both cases correspond to statistically steady regimes. Nonetheless, the case corresponding to the less intense forcing ( $t_A/t_p = 0.1$  in Figure 8a), shows a comparatively fewer number of current sheets. Therefore, the number of current sheets seems to be controlled by the intensity of the forcing. The widths of these current sheets on the other hand, are mostly determined by the dynamics. As a result, in both cases a wide range of current sheet widths can be observed.

## VII. CONCLUSIONS

We presented results of the turbulent dynamics of a bundle of magnetic flux ropes driven at their endpoints with steady convective motions. Two dimensionless parameters controlling the response of the system are identified: the dissipation coefficient and the ratio between the Alfvén wave box crossing time to the forcing timescale,  $t_A/t_p$ . As we showed in a previous work [25], the dissipation rate strongly depends on the value of this timescale ratio, and is only weakly dependent on the dissipation coefficient. It is found that the external driving generates a broadband perpendicular energy spectrum with a slope which is determined by the timescale ratio  $t_A/t_p$ . For small values of this ratio, a spectrum with slope  $\alpha \approx -2.4$  is obtained. For  $t_A/t_p \sim 0.5$  the spectrum is  $\sim k_\perp^{-2}$ , which would indicate a realization of the regime known as weak turbulence. For higher values of  $t_A/t_p$  the spectrum approaches the Kolmogorov form  $k_\perp^{-5/3}$ . Both the weak turbulent and the Kolmogorov spectra can be obtained from a common phenomenological framework based on the assumed value of the time for decay of triple correlations. The regime corresponding to spectral power laws with slope -2.4 and lower for low values of  $t_A/t_p$  should be attributed to the relatively small amplitude flow at the boundaries. The phenomenological framework can be modified to consider this weak velocity field case and a steep magnetic spectrum  $\sim k_\perp^{-3}$  is obtained. We also show the development of small scale spatial structures, in the form of current sheets oriented along the mean field. The number of current sheets seems to be controlled by the timescale ratio  $t_A/t_p$ , while the widths of these current sheets on the other hand, are mostly determined by the dynamics. A wide range of current sheet widths can be observed. The system presented here should be considered as an example of the effect of the boundaries on MHD turbulence. To our knowledge, there is a lack of such studies in the literature and further investigation along these lines should be extended to other MHD systems (3D MHD, compressible) as well.

## **ACKNOWLEDGMENTS**

Research supported by NASA NAG5-7164, NSF ATM-0105254 and ATM-9977692. DOG is a researcher of CONICET (Argentina) and acknowledges support from grants UBACYT X209 (University of Buenos Aires, Argentina) and PICT 03-9483 (ANPCyT, Argentina).

## REFERENCES

- [1] A.N. Kolmogorov, Dokl. Acad. Sci. URSS, 30, 301 (1941)
- [2] P.S. Iroshnikov, Astron. Zh., **40**, 742 (1963)
- [3] R. Kraichnan, *Phys. Fluids*, 8, 1385 (1965)
- [4] D. Fyfe, D. Montgomery, & G. Joyce, J. Plasma Phys. **17**, 369 (1977)
- [5] W.H. Matthaeus, & Y. Zhou, Phys. Fluids B **1**, 1929 (1989)
- [6] W.-C. Muller, & D. Biskamp, Phys. Rev. Lett. **84**, 475 (2000)
- [7] J.V. Shebalin, W.H. Matthaeus, & D. Montgomery, J. Plasma Phys. **29**, 525 (1983)
- [8] S. Oughton, E.R. Priest, & W.H. Matthaeus, J. Fluid Mech. **280**, 95 (1994)
- [9] P. Goldreich, & S. Sridhar, *Astrophys. J.* **485**, 680 (1997)
- [10] R. Kinney, & J.C. McWilliams, Phys. Rev. E **57**, 7111 (1998)
- [11] W.H. Matthaeus, S. Ghosh, S. Oughton, & D.A. Roberts, J. Geophys. Res. **101**, 7619 (1996)
- [12] G. P. Zank, & W.H. Matthaeus, J. Plasma Phys. **48**, 85 (1992)
- [13] H. Strauss, Phys. Fluids, 19, 134 (1976)
- [14] D.C. Montgomery, Phys. Scr. **T2/1**, 83 (1982)
- [15] C. S. Ng, & A. Bhattacharjee, Phys. Plasmas **4**, 605 (1997)
- [16] S. Galtier, S.V. Nazarenko, A.C. Newell, & A. Pouquet, J. Plasma Phys. **63**, 447 (2000)
- [17] E.N. Parker, *Astrophys. J.* **174**, 499 (1972)
- [18] A.A. van Ballegooijen, *Astrophys. J.* **311**, 1001 (1986)
- [19] D.W. Longcope, & R.N. Sudan, *Astrophys. J.*, 437, 491 (1994)

- [20] Z. Mikić, D.D. Schnack, & G. van Hoven, *Astrophys. J.*, 338, 1148 (1989)
- [21] D.L. Hendrix, & G. Van Hoven, *Astrophys. J.*, 467, 887 (1996)
- [22] L. Milano, P. Dmitruk, C. Mandrini, D.O. Gómez, & P. Demoulin, *Astrophys. J.*, 521, 889 (1999)
- [23] D.O. Gómez, & C. Ferro Fontán, *Astrophys. J.*, 394, 662 (1992)
- [24] K. Galsgaard, & A. Nordlund, *J. Geophys. Res.* bf 101, 13445 (1996)
- [25] P. Dmitruk, & D.O. Gómez, *Astrophys. J.*, 527, L63 (1999)
- [26] C.H. Mandrini, P. Demoulin, & J.A. Klimchuk, *Astrophys. J.*, **530**, 999 (2000)
- [27] C. Canuto, M.Y. Hussaini, A. Quarteroni, & T.A. Zang, *Spectral Methods in Fluid Dynamics* (Springer, New York, USA, 1988), 1.
- [28] D.L. Hendrix, G. Van Hoven, Z. Mikic, & D.D. Schnack, *Astrophys. J.* **470**, 1192 (1996)
- [29] K.R. Sreenivasan, *Phys. Fluids* **27**, 1048 (1984)
- [30] G. K. Batchelor, *The theory of homogeneous turbulence*, Cambridge University Press (Cambridge, UK, 1953), 106.
- [31] U. Frisch, *Turbulence*, Cambridge Univ. Press (Cambridge, UK, 1996), 69.
- [32] A. Bhattacharjee, C.S. Ng, *Astrophys. J.* **548**, 318 (2001)
- [33] Y. Zhou, *Phys. Fluids* **7**, 2092 (1995)
- [34] R. Grappin, A. Pouquet, and J. Léorat, *Astron. Astrophys.* **126**, 51 (1983)



## FIGURES

FIG. 1. Cartoon of the reduced MHD setup.

FIG. 2. Top: magnetic and kinetic energy (dashed) vs time from a run with  $S = 2000$ ,  $t_A/t_p = 0.5$ . Bottom: Dissipation rate and forcing (dashed) for the same run.

FIG. 3. Perpendicular energy spectra from  $S = 2000$  runs and different values of the ratio  $t_A/t_p = 0.1, 0.5, 1$ . Resolution is  $1024 \times 1024 \times 64$ ,  $2048 \times 2048 \times 64$ ,  $2048 \times 2048 \times 128$  respectively. On the left panels, magnetic and kinetic energy (dashed) perpendicular spectra. The dotted lines show exact power laws given for reference. On the right, total “compensated” perpendicular spectra and corresponding power index value  $\alpha$ .

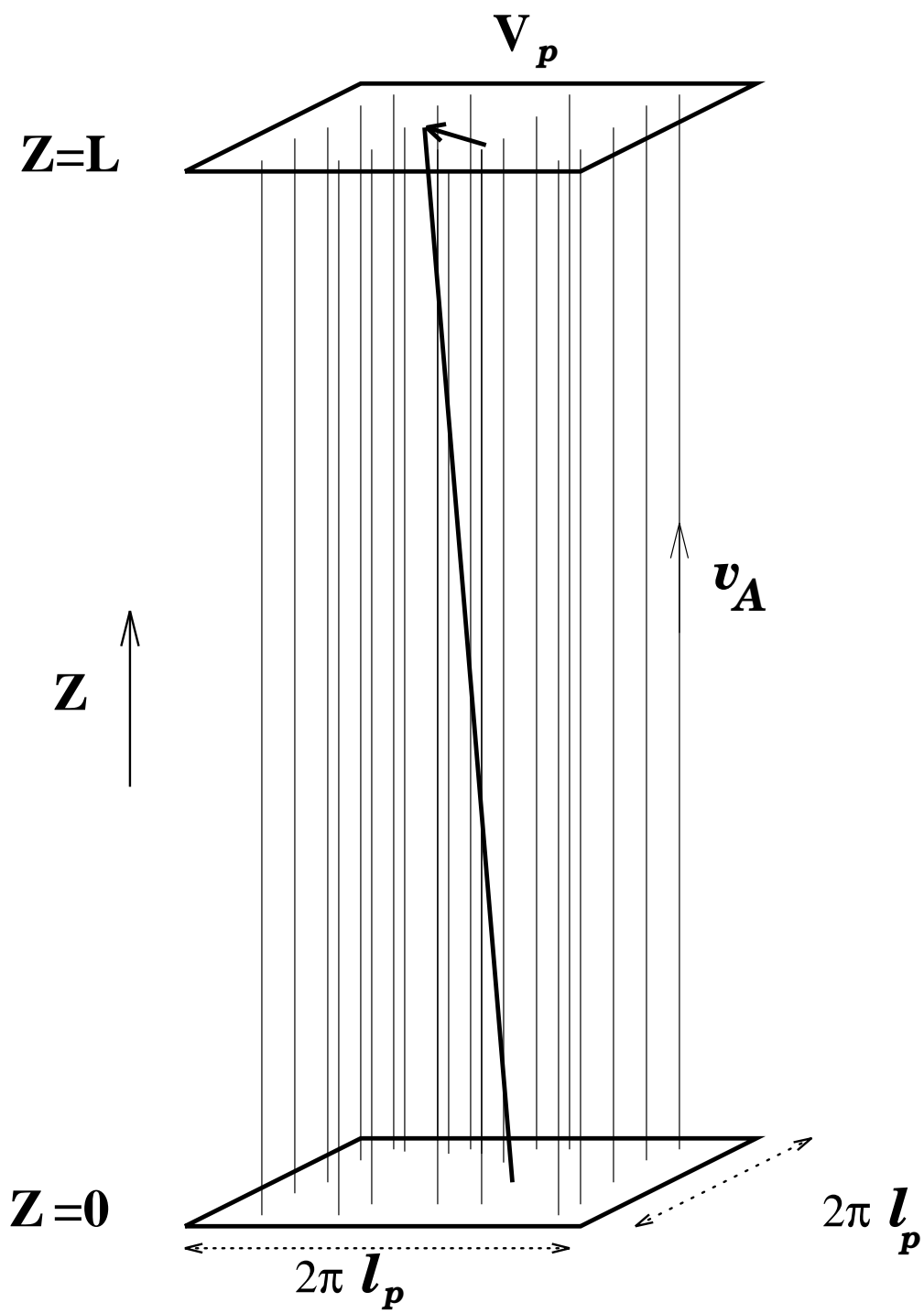
FIG. 4. Spectra and compensated spectra for a run with  $S = 800$ ,  $t_A/t_p = 2$ .

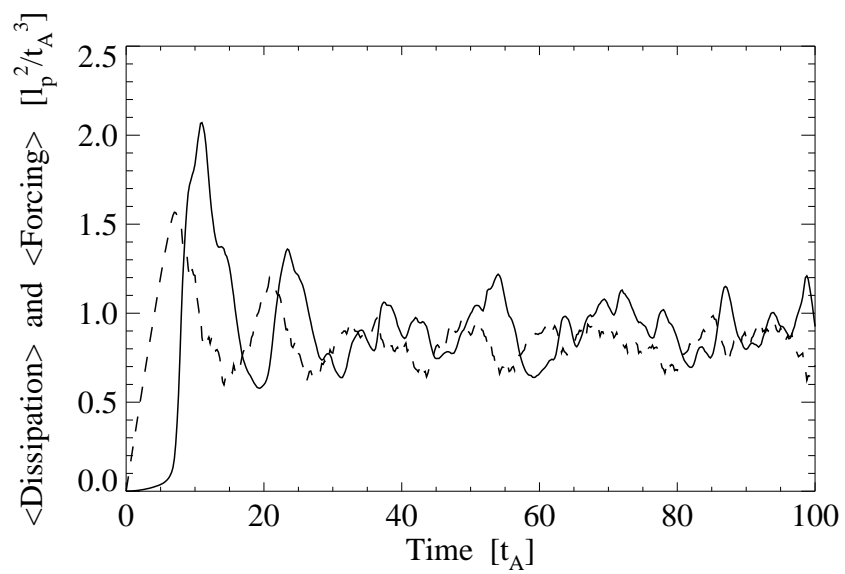
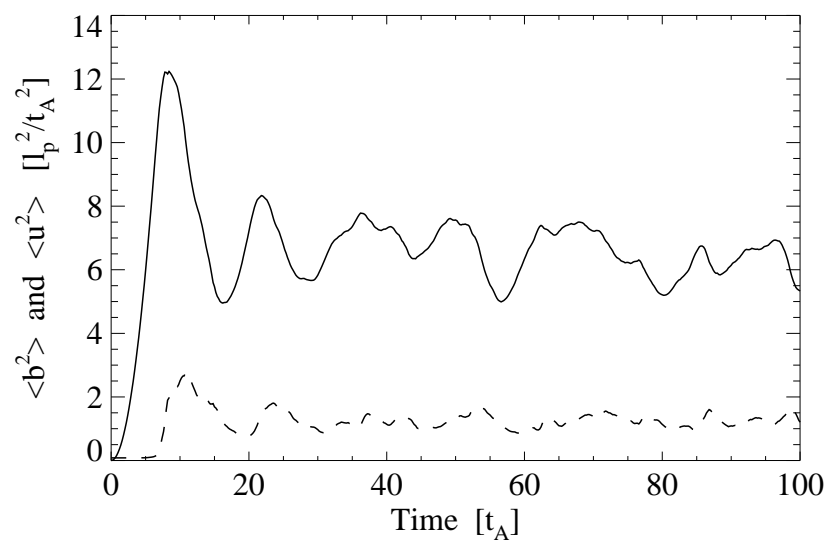
FIG. 5. Perpendicular energy spectra for the Elsasser fields  $\mathbf{z}^\pm$  from  $S = 2000$  runs and different values of the ratio  $t_A/t_p = 0.1, 0.5, 1$ . On the left panels,  $E_{k_\perp}^+$  and  $E_{k_\perp}^-$  (dashed) spectra. On the right, compensated spectra for the product  $E_{k_\perp}^+ E_{k_\perp}^-$  and corresponding power index value  $\alpha$ .

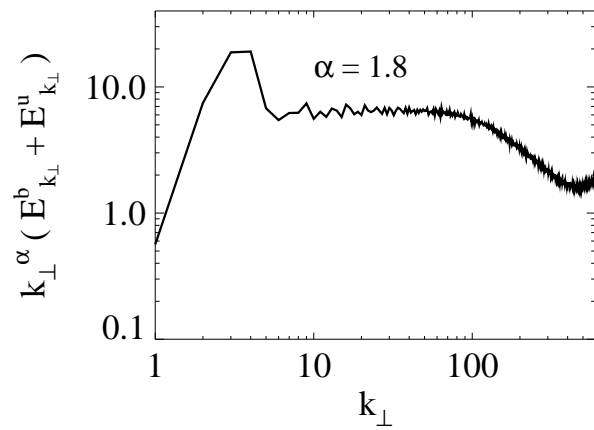
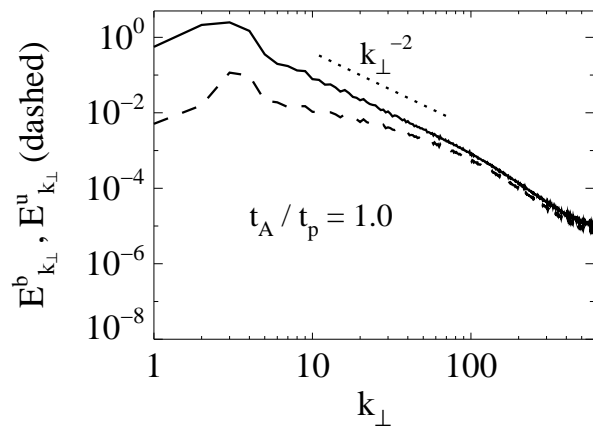
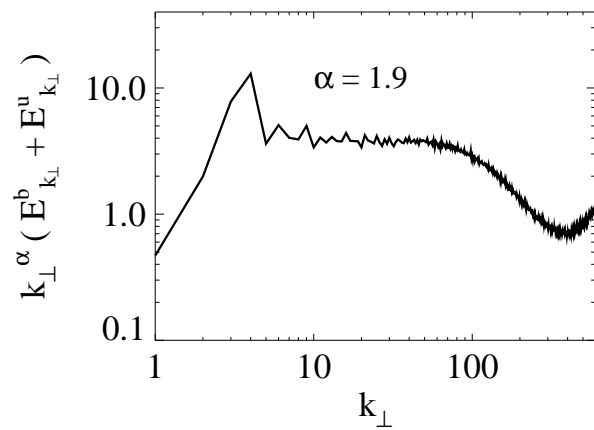
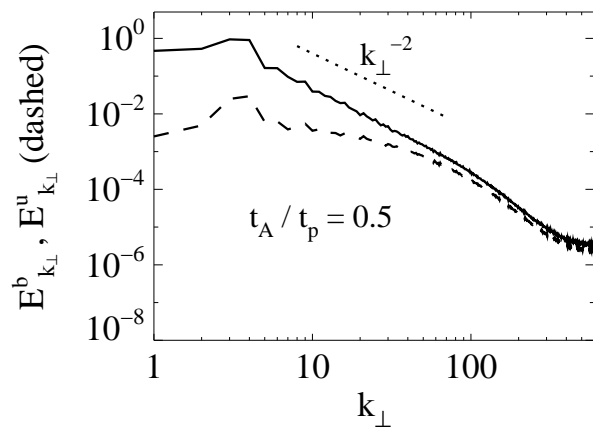
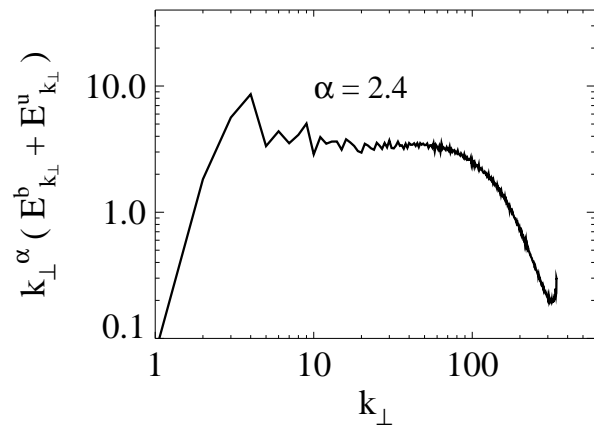
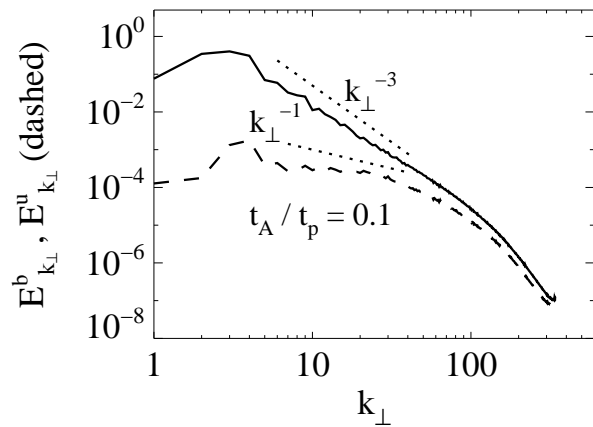
FIG. 6. The  $k$ -dependent kinetic Reynolds number  $R_k = u_k/(k \nu) = \sqrt{(E_k^u/k)}/\nu$  for a run with  $S = 2000$ ,  $t_A/t_p = 1$ .

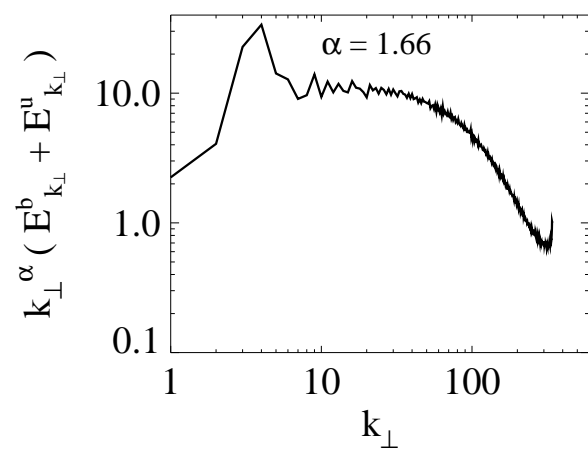
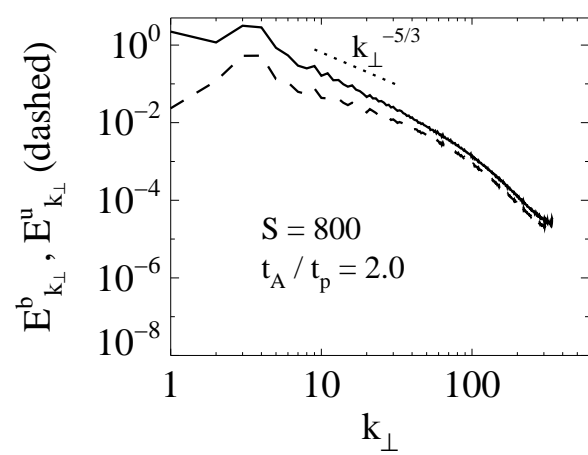
FIG. 7. Resolution study of the spectra for runs with  $S = 2000$ ,  $t_A/t_p = 0.1$

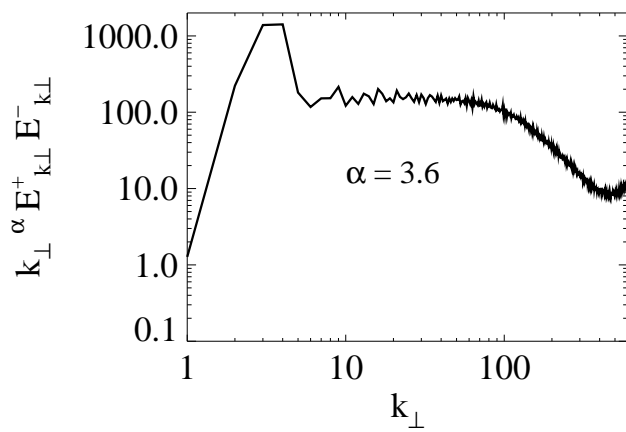
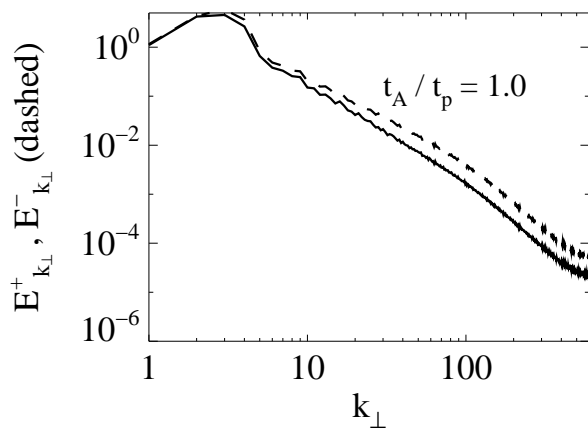
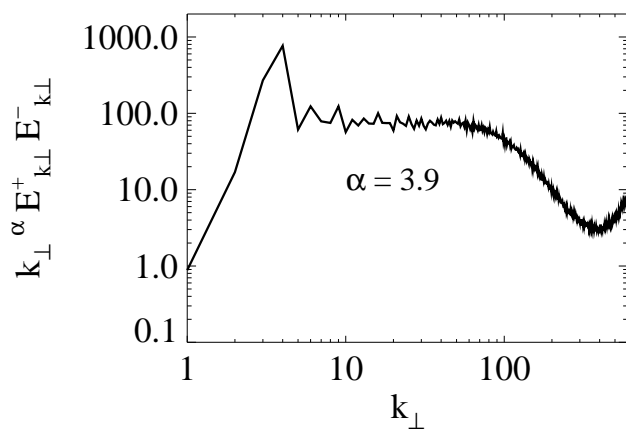
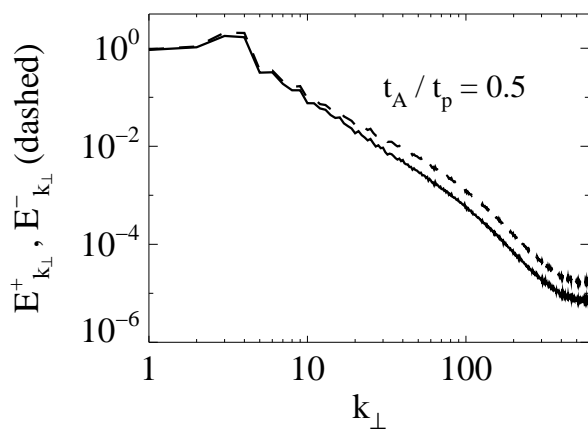
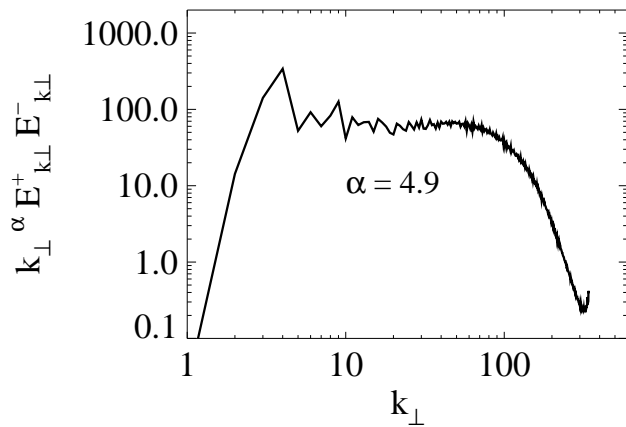
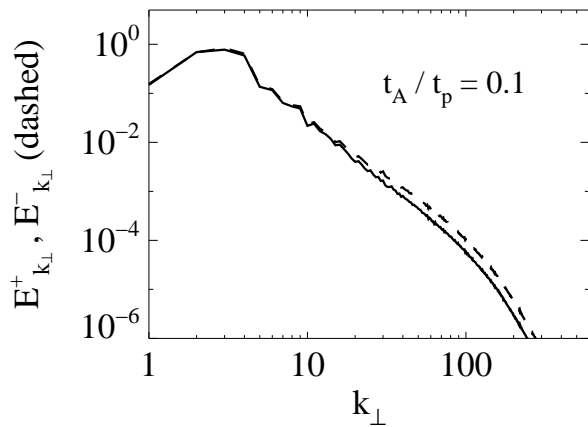
FIG. 8. Cross section of parallel current density for cases with  $t_A/t_p = 0.1$  and  $t_A/t_p = 0.5$ .

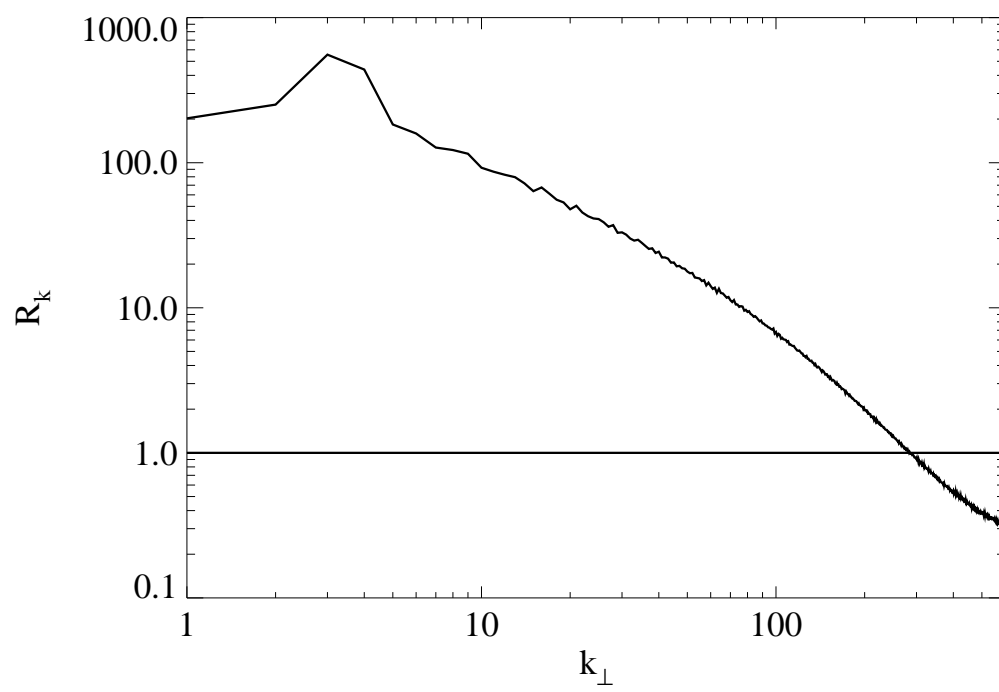


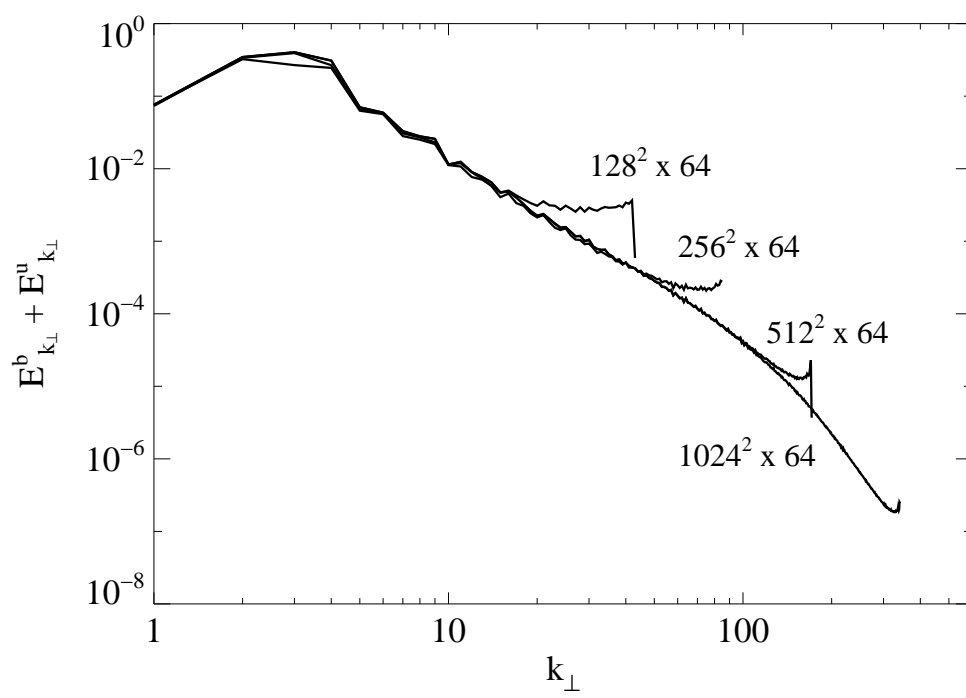






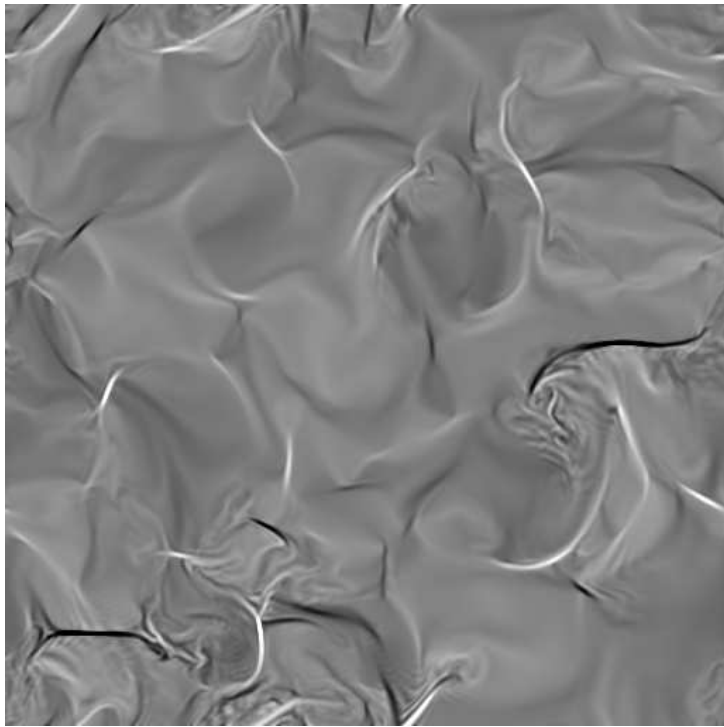








$$t_A/t_p=0.1$$



$$t_A/t_p=0.5$$

